

Magnetic Field Effects in Frustrated Low-dimensional Magnets

Burkhard Schmidt, Mohammad Siahatgar, and Peter Thalmeier

We present recent results from our investigation of the frustrated two-dimensional $S = 1/2$ next nearest neighbor anisotropic Heisenberg antiferromagnet on a square lattice as described by the $J_{1a,b}$ - J_2 model [1, 2]. This model has a number of realizations in layered V^{4+} compounds [3–5]. Combining the results of several experimental investigations, the determination of the location of these compounds in the phase diagram was possible [6–8]. It was eventually found that all known compounds are lying in the region of columnar antiferromagnetic order, characterized by an ordering vector $\vec{Q} = (\pi, 0)$ or $(0, \pi)$. Strictly speaking, the V^{4+} compounds all have slight orthorhombic distortions, leading to a spatial anisotropy in the nearest-neighbor exchange constants J_{1a} and J_{1b} along the respective crystallographic directions.

Recently, results from inelastic neutron scattering (INS) on the low-energy excitations of the 122 Fe pnictides have shown that these can also be described by a local-moment model with nearest- and next-nearest neighbor exchange integrals, despite the metallic nature of these compounds [9–12]. Here, a spatial anisotropy of the exchange parameters has been introduced, too.

INS results also show that in the Fe pnictides, well-defined spin excitations exist in the whole Brillouin zone, which suggests a local-moment picture for the magnetic excitations to be applicable. The experimentally observed size of the ordered moment is strongly reduced compared to predictions from density-functional theory. In this report, we summarize our results on the anisotropic frustrated two-dimensional $S = 1/2$ Heisenberg model on the square (or better rectangular) lattice. Within this model, it seems natural to investigate to what extent frustration can serve as an origin for the observed moment reduction.

The Hamiltonian we discuss has the form

$$H = \sum_{\langle ij \rangle} J_{ij} \vec{S}_i \vec{S}_j - g\mu_B H \sum_i S_i^z, \quad (1)$$

where $J_{ij} = \text{diag}(J_{ij}^\perp, J_{ij}^\perp, J_{ij}^z)$, and $J_{ij} = J_{1a}$ or J_{1b} if i and j mark nearest-neighbor sites along the crystallographic a and b directions, respectively, $J_{ij} = J_2$ if i and j denote next-nearest neighbors, and the

sum runs over all nearest- and next-nearest neighbor bonds. The magnetic field $\vec{h} = g\mu_B \vec{H}$ points along the z direction in spin space. On each site i , we introduce a local coordinate system, where the z axis is oriented parallel to the local magnetic moment, and express the spin operator products in Eq. (1) in these coordinates.

For the classical ground-state energy, we get

$$E_{\text{cl}} = NS^2 \left[J_\perp(\vec{Q}) - A(0) \cos^2 \Theta_c \right] \quad (2)$$

where $J_\perp(\vec{Q})$ is the Fourier transform of the exchange constants perpendicular to the magnetic field, Θ_c is the canting angle of the spins with respect to the magnetic field given by $\cos \Theta_c = h/[2SA(0)]$, and

$$A(\vec{k}) = J_z(\vec{k}) + \frac{1}{2} \left[J_\perp(\vec{k} + \vec{Q}) + J_\perp(\vec{k} - \vec{Q}) \right] - 2J_\perp(\vec{Q}). \quad (3)$$

Minimizing $E_{\text{cl}}(\vec{Q})$ with respect to \vec{Q} yields the ordering vector \vec{Q} .

Linear spin-wave theory

Within the framework of linear spin-wave theory, we expand the Hamiltonian around its classical limit up to first order in $1/S$. The result is

$$\mathcal{H} = E_{\text{cl}} + E_{\text{zp}} + S \sum_{\vec{k}} E(h, \vec{k}) \alpha_{\vec{k}}^\dagger \alpha_{\vec{k}}, \quad (4)$$

where E_{cl} is given by Eq. (2),

$$E_{\text{zp}} = NSJ_\perp(\vec{Q}) + \frac{S}{2} \sum_{\vec{k}} E(h, \vec{k}) \quad (5)$$

is the zero-point energy contribution to the total ground state energy, and $E(h, \vec{k})$ is the field-dependent excitation energy of a magnon with momentum \vec{k} , which is of the form

$$E(h, \vec{k}) = \left\{ \left[A(\vec{k}) - B(\vec{k}) \cos^2 \Theta_c \right]^2 - \left[B(\vec{k}) (1 - \cos^2 \Theta_c) \right]^2 \right\}^{1/2}$$

$$\begin{aligned}
 & + C(\vec{k}) \cos \Theta_c, \quad (6) \\
 B(\vec{k}) & = J_z(\vec{k}) - \frac{1}{2} \left(J_\perp(\vec{k} + \vec{Q}) + J_\perp(\vec{k} - \vec{Q}) \right), \\
 C(\vec{k}) & = J_\perp(\vec{k} + \vec{Q}) - J_\perp(\vec{k} - \vec{Q}).
 \end{aligned}$$

The ordered moment M is the ground-state expectation value of the z component of the spin \vec{S} in local coordinates and can be expressed as

$$M = S \left[1 - \frac{1}{2S} \left(\frac{1}{N} \sum_{\vec{k}} \frac{A(\vec{k}) - B(\vec{k}) \cos^2 \Theta_c}{E(h, \vec{k})} - 1 \right) \right] \quad (7)$$

in units of $g\mu_B$. Due to quantum fluctuations $M < S$ is smaller than in the classical case, except for the ferromagnet, which is an eigenstate of the Hamiltonian.

In a similar way we can express the magnetization m as the z component of the spin \vec{S} in the *global* coordinate system, which is equivalent to a projection of the ordered moment onto the direction of the magnetic field. We get

$$m = S \cos \Theta_c \left[1 + \frac{1}{2S} \frac{1}{N} \sum_{\vec{k}} \frac{B(\vec{k}) (A(\vec{k}) - B(\vec{k}))}{A(0)E(h, \vec{k})} \right], \quad (8)$$

in units of $g\mu_B$, again up to first order in $1/S$.

We note that the results presented in this section are in no way specific to the $J_{1a,b}-J_2$ model, but apply to arbitrary spin Hamiltonians on Bravais lattices, provided the presence of the applied magnetic field does not destroy the $U(1)$ spin symmetry assumed here.

Exact diagonalization

We have also developed a new finite-size scaling method applied to exact-diagonalization data obtained from diagonalizing the Hamiltonian matrix derived from Eq. (1) on small clusters, providing us with an—apart from the small tile size—unbiased method to determine the ground-state properties of the model.

For a unique description of the lattice tiling, we use matrices in *hermite normal form* (HNF),

$$H = \begin{pmatrix} h_{11} & h_{12} \\ 0 & h_{22} \end{pmatrix} \quad (9)$$

with integer h_{ij} representing tiles with the special edge vectors $\vec{h}_1 = (h_{11}, h_{12})$ and $\vec{h}_2 = (0, h_{22})$ and area or number of sites $N = h_{11}h_{22}$.

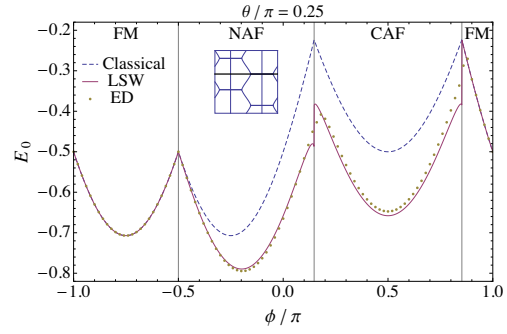


Fig. 1: The ground-state energy as function of the frustration angle ϕ for the isotropic model with fixed $\theta = \pi/4$. The classical energy is shown as dashed line, and the spin-wave results including zero-point fluctuations are presented as solid line. Dots indicate the values for the ground-state energy obtained from extrapolating our exact-diagonalization data. The inset shows a sketch of the classical phase diagram as a function of ϕ and θ .

Secondly, we introduce the *compactness* or *squareness* of a tile,

$$\rho = \frac{4 \times \text{area}}{\text{perimeter}^2}, \quad (10)$$

which is to be determined from the area and circumference of the most compact tile out of the class of tiles represented by the HNF matrix H .

With this scheme, we find 816 different classes of tiles with area N between 8 and 32.

The classical $J_{1a,b}-J_2$ model on the square lattice has four ground states with ordering wave vectors $\vec{Q} = (0, 0)$, (π, π) , and $\vec{Q} = (\pi, 0)$ or $(0, \pi)$, the corresponding phases we abbreviate with FM, NAF, CAFa, and CAFb, respectively. Although in the quantum case the corresponding wave functions, except for the ferromagnet, are not eigenstates of the Hamiltonian, it is important that the tilings of the infinite lattice are chosen such that these states corresponding to the classically ordered phases are not suppressed when applying periodic boundary conditions. We therefore select, for each even tile area and for each classical phase, the tile having the maximum squareness to be included into the finite-size scaling analysis.

The ordered moment, which is strictly speaking a property of the infinite lattice only, can be obtained indirectly from the static structure factor

$$S_N(\vec{Q}) = \frac{1}{\mathcal{N}} \sum_{i,j=1}^N \langle \vec{S}_i \vec{S}_j \rangle e^{i\vec{Q} \cdot (\vec{R}_i - \vec{R}_j)}, \quad (11)$$

$$M^2(\vec{Q}) = \lim_{N \rightarrow \infty} S_N(\vec{Q}), \quad (12)$$

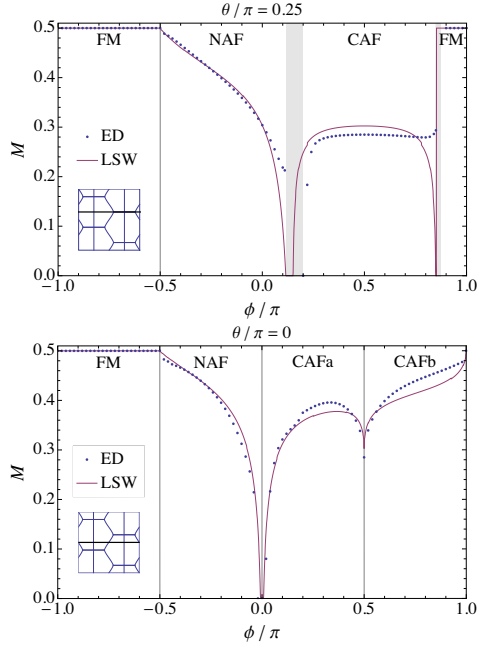


Fig. 2: The extrapolated ordered moment as function of the frustration angle, for (top) the isotropic $\theta = \pi/4$ case and (bottom) the maximally anisotropic case with $\theta = 0$. The gray-shaded areas in the top plot represent the range of frustration angles ϕ where the relative error of $M^2(\vec{Q})$ is above 0.1.

where we set $\mathcal{N} = N(N + 1/S)$, and independently from the long-distance correlation function

$$\lim_{|\vec{R}_i - \vec{R}_j| \rightarrow \infty} \left| \langle \vec{S}_i \vec{S}_j \rangle \right| = \left| \langle \vec{S}_i \rangle \langle \vec{S}_j \rangle \right| = M^2(\vec{Q}). \quad (13)$$

Results

We parameterize the exchange constants according to

$$\begin{aligned} J_{1a} &= \sqrt{2}J_c \cos \phi \cos \theta, \\ J_{1b} &= \sqrt{2}J_c \cos \phi \sin \theta, \\ J_2 &= J_c \sin \phi, \\ J_c &= \sqrt{\frac{1}{2} (J_{1a}^2 + J_{1b}^2) + J_2^2}, \end{aligned} \quad (14)$$

introducing an energy scale J_c , a frustration angle ϕ and an anisotropy ratio θ (not to be confused with the canting angle Θ_c).

Fig. 1 displays the ground-state energy as a function of the frustration angle ϕ for the isotropic $J_{1a} = J_{1b}$ case with $\theta = \pi/4$. The dotted line displays the classical ground-state energy obtained from Eq. (2), the solid line shows the result from linear spin-wave theory, Eq. (4). Dots denote the values obtained

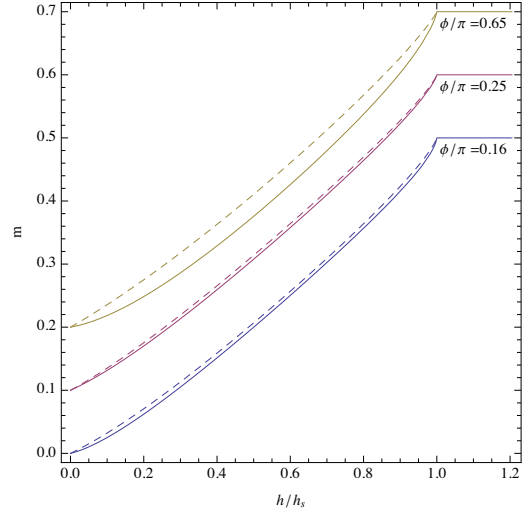


Fig. 3: Uniform magnetic moment m per site as a function of the applied magnetic field h normalized to the saturation field $h_s = 2SA(0)$ at three different frustration angles in the CAF phases, $\phi/\pi = 0.16$ (near NAF), 0.25 (CAF_a), and 0.65 (CAF_b near FM). Between each pair of adjacent curves an offset $\Delta m = 0.1$ is inserted. The solid lines denote the field dependence in the isotropic case, $\theta = \pi/4$, the dashed lines denote the maximally anisotropic case, $\theta = 0$.

from extrapolating our exact-diagonalization data to the thermodynamic limit. The agreement between linear spin-wave theory and exact diagonalization is remarkably well, apart from the regions around the classical borders of the CAF phase.

Fig. 2 shows the dependence of the ordered moment on the frustration angle ϕ , again for the isotropic model with $\theta = \pi/4$ in the top part, and for the anisotropic model with $\theta = 0$ at the bottom. The solid lines denote the results from linear spin-wave theory, Eq. (7), the dots represent the extrapolated values derived from the structure factor according to Eq. (11). Compared to the classical, constant value $M_{cl} = S = 1/2$, the ordered moment is strongly reduced due to enhanced quantum fluctuations already at moderate frustration. In fact M vanishes around the classical borders of the columnar phase, indicating the emergence of two nonmagnetic phases not discussed here. However, introducing a spatial anisotropy ($\theta \neq \pi/4$) lifts the degeneracy between the two columnar phases CAF_a and CAF_b and *stabilizes* the ordered moment.

A similar effect can be observed in the field dependence of the uniform magnetization m , Eq. (8) shown in Fig. 3 for three different values of the frustration parameter ϕ . The solid lines in the plot denote $m(h)$ for the isotropic model [13]. In particular near the crossover to the nonmagnetic re-

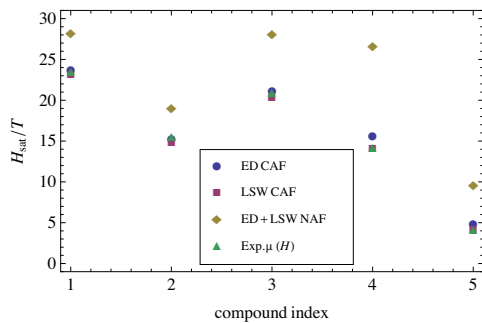


Fig. 4: Comparison of saturation fields predicted by exact diagonalization (ED, dots and diamonds) and spin-wave theory (LSW, squares and diamonds), and determined from high-field experiments [14] (triangles). The compounds are (1) $\text{PbZnVO}(\text{PO}_4)_2$, (2) $\text{Na}_{1.5}\text{VOPO}_4\text{F}_{0.5}$, (3) $\text{Pb}_2\text{VO}(\text{PO}_4)_2$, (4) $\text{SrZnVO}(\text{PO}_4)_2$, and (5) $\text{BaCdVO}(\text{PO}_4)_2$. The agreement with the saturation fields for the columnar phase (CAF) is very good, giving a direct proof that all compounds investigated undergo columnar ordering at low temperatures.

gions, the curves are strongly nonlinear, suppressed from the classical linear behavior $m_{\text{cl}} = Sh/h_s$ for $h \leq h_s = 2SA(0)$. This effect, which is due to zero-point fluctuations of the ground state, too, is reduced when introducing a spatial anisotropy, see the dotted lines in the figure.

Fig. 4 displays a comparison of the saturation fields predicted by exact diagonalization and spin-wave theory for the columnar and Néel antiferromagnetic phases with the observed experimental values derived from high-field measurements for five different V^{4+} compounds. The predicted theoretical values are based on fits of our exact-diagonalization data and of a high-temperature series expansion [14–16] to the temperature dependences of the low-field susceptibilities. The experiments agree surprisingly well with the predicted CAF values, demonstrating that all compounds order in a columnar magnetic structure at low temperatures.

Summary

We have done an extensive analysis of the $J_{1a,b}$ - J_2 model both with linear spin-wave theory and numerical exact diagonalization. The agreement between the two approaches was found to be generally good, and both methods predict the strong suppression and eventual breakdown of the ordered moment in the transition regions at the borders of the columnar phases as a function of frustration. A spatial anisotropy has a stabilizing effect on the ordered

moment in the columnar phases. Subject of current investigations are quantitative analysis of an increase of the three-dimensional magnetic ordering temperature T_N in finite fields, reflected in a field-induced stabilization of the ordered moment, which was recently observed in $\text{Cu}(\text{pz})_2(\text{ClO}_4)_2$ [17].

References

- [1] B. Schmidt, M. Siahatgar, and P. Thalmeier, Phys. Rev. B **81** (2010) 165101.
- [2] B. Schmidt, M. Siahatgar, and P. Thalmeier, Phys. Rev. B **83** (2011) 075123.
- [3] E. E. Kaul, H. Rosner, N. Shannon, R. V. Shpanchenko, and C. Geibel, J. Magn. Magn. Mat. **272-276** (2004) 922.
- [4] N. S. Kini, E. E. Kaul, and C. Geibel, J. Phys.: Cond. Mat. **18** (2006) 1303.
- [5] A. A. Tsirlin and H. Rosner, Phys. Rev. B **79** (2009) 214417.
- [6] N. Shannon, B. Schmidt, K. Penc, and P. Thalmeier, Eur. Phys. J. B **38** (2004) 599.
- [7] B. Schmidt, P. Thalmeier, and N. Shannon, Phys. Rev. B **76** (2007) 125113.
- [8] B. Schmidt, M. Siahatgar, P. Thalmeier, and A. A. Tsirlin, J. Phys.: Conf. Ser. **200** (2010) 022055.
- [9] R. A. Ewings, T. G. Perring, R. I. Bewley, T. Guidi, M. J. Pitcher, D. R. Parker, S. J. Clarke, and A. T. Boothroyd, Phys. Rev. B **78** (2008) 220501(R).
- [10] R. J. McQueeney, S. O. Diallo, V. P. Antropov, G. D. Samolyuk, C. Broholm, N. Ni, S. Nandi, M. Yethiraj, J. L. Zarestky, J. J. Pulikkotil, A. Kreyssig, M. D. Lumsden, B. N. Harmon, P. C. Canfield, and A. I. Goldman, Phys. Rev. Lett. **101** (2008) 227205.
- [11] S. O. Diallo, V. P. Antropov, T. G. Perring, C. Broholm, J. J. Pulikkotil, N. Ni, S. L. Bud'ko, P. C. Canfield, A. Kreyssig, A. I. Goldman, and R. J. McQueeney, Phys. Rev. Lett. **102** (2009) 187206.
- [12] J. Zhao, D. T. Adroja, D.-X. Yao, R. Bewley, S. Li, X. F. Wang, G. Wu, X. H. Chen, J. Hu, and P. Dai, Nat. Phys. **5** (2009) 555.
- [13] P. Thalmeier, M. E. Zhitomirsky, B. Schmidt, and N. Shannon, Phys. Rev. B **77** (2008) 104441.
- [14] A. A. Tsirlin, B. Schmidt, Y. Skourski, R. Nath, C. Geibel, and H. Rosner, Phys. Rev. B **80** (2009) 132407.
- [15] R. Nath, A. A. Tsirlin, H. Rosner, and C. Geibel, Phys. Rev. B **78** (2008) 064422.
- [16] H. Rosner, R. R. P. Singh, W. H. Zheng, J. Oitmaa, and W. E. Pickett, Phys. Rev. B **67** (2003) 014416.
- [17] N. Tsyrlin, F. Xiao, A. Schmeidewind, P. Link, H. M. Rønnow, J. Gavilano, C. P. Landee, M. M. Turnbull, and M. Kenzelmann, Phys. Rev. B **81** (2010) 134409.